Numerical Heat Transfer, Part A, vol. 24, pp. 229–247, 1993

A COMPARATIVE ANALYSIS OF FINITE ELEMENT AND FINITE DIFFERENCE METHODS FOR FREE SURFACE TRANSPORT

S. C. Chen and K. Vafai
Department of Mechanical Engineering, Ohio State University, Columbus, Ohio 43210

The present work consists of the comparative evaluation of the finite element method (FEM) and the finite difference method (FDM) for the analysis of free surface transport within a hollow ampule. The phenomenon of motion reversal of the free surfaces obtained earlier by the FDM is also analyzed by the FEM. It is found that the times at which the motion reversal occurs are independent of the applied pressure difference for any fixed dimension of the hollow ampule. Furthermore, it appears that the displacement of the inner and outer free surfaces varies linearly with the magnitude of the applied pressure difference. Finally, detailed comparative discussion is presented on the differences between the results obtained by FDM and FEM.

INTRODUCTION

In an earlier work, Vafai and Chen [1] analyzed free surface transport within a hollow ampule using the finite difference method (FDM). That same hollow ampule configuration (Fig. 1) is analyzed in this work. The hollow ampule is essentially composed of a circular thin film with rigid top and bottom ends. The ampule's motion is produced by the pressure difference between the inner and outer surfaces. This pressure difference can be induced by any type of heat source striking the outer surface, for example, the thermal radiation pressure that is induced by the radiation heat source striking on the outer free surface [1, 2]. These aspects were discussed in more detail in Vafai and Chen [1].

The material chosen for the present analysis is glass, because glass and ceramic materials have become extremely useful in a variety of applications in the last few decades. In the electronic industry, glass is probably the most familiar of all insulating materials. For example, central to understanding and optimization of hermetic type sealing used in various electronic applications is the accurate prediction of free surface transport within a hollow glass ampule. It should be noted that the present work constitutes a generic investigation of free surface transport.

Most of the FDM free surface investigations are based on the marker-and-cell (MAC) method or its variant. This method, which solves the incompressible transient flow equations using primitive variables, as explained in detail in [1], was originally developed at the Los Alamos National Laboratory. Other numerical techniques dealing with different types of free boundary problems have been developed since the introduction of the MAC method, as explained in Vafai and Chen [1].

1040–7782/93 $10.00 + .00

NOMENCLATURE

D_i	inner diameter of the hollow ampule, m
D_o	outer diameter of the hollow ampule, m
H	height of the hollow ampule
p	pressure, Pa
p^h	FEM approximation for pressure, Pa
R_i	inner radius of the hollow ampule, m
R_o	outer radius of the hollow ampule, m
r, z	radial and axial cylindrical coordinates, m
t	time, s
Δt	time increment, s
u_r, u	velocity in the r direction, ms^{-1}
u_z, v	velocity in the z direction, ms^{-1}
u_r^h	FEM approximation for the r component of velocity, ms^{-1}
u_z^h	FEM approximation for the z component of velocity, ms^{-1}
V	column vector consisting of all the unknown variables in the computational domain (u_r, u_z, p)
η	refers to the inner free surface
ξ	refers to the outer free surface

Subscripts

i	index for r direction or inner free surface
j	index for z direction or outer free surface
N	index for time step
o	outer free surface
r	r component
z	z-component

Superscripts

T	transpose of a matrix

The work by Vafai and Chen [1] constitutes one of the first investigations on free surface problems related to cylindrical coordinates that includes full consideration of the free surface boundary conditions. In that work, the Navier-Stokes equations in cylindrical coordinates were discretized using a semi-implicit finite difference scheme with full consideration of the surface tension effects along with normal and tangential boundary conditions on both free surfaces. In this work, both the FDM and finite element method (FEM) have been used to obtain a critical comparison between these two methods for free surface problems. The FEM, while enjoying widespread use in structural problems, has a relatively short history in computational fluid mechanics.

In recent years, however, various research has shown convincingly that FEM is a powerful tool in fluid mechanics. A positive aspect of FEM is its inherent flexibility in treating arbitrarily complex flow domains and boundary conditions. Unstructured grids can be designed that allow areas of interest to be studied in great detail without the need for excessive grid points throughout the entire flow domain. FEM allows the natural and correct imposition of boundary conditions on curved boundaries, which is a very important consideration in the present study, where free surfaces are involved in the computational domain. Furthermore, the FEM formulation allows for an easier derivation of comprehensive error estimates and the determination of accurate solutions.

Despite the fact that the FEM is becoming a popular numerical tool in the solution of fluid mechanics and heat transfer problems, very limited work has been done in the way of assessing the accuracy and differences between the FEM and

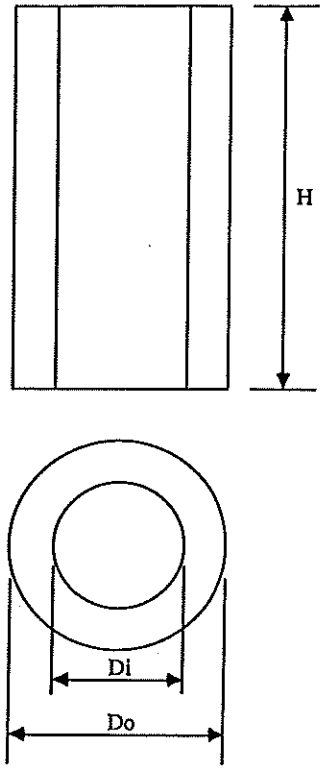

Fig. 1 Schematic diagram of the hollow ampule.

FDM for situations other than conduction type problems. In particular, there appears to be no comparison between the two methods for free surface problems. The work done by Wang [3] on the free surface problem involved in the glass tube sealing process is one of the only FEM works in this area. However, that work was restricted to a one-dimensional simplification in the cylindrical coordinate. It is clear that there is a definitive need for a comparative and complete analysis of these two methods for free surface flow and heat transfer problems.

The present study provides such a comparative evaluation of the FDM and FEM for free surface fluid flow. Specifically, in this work the free surface fluid flow inside a hollow ampule is investigated using both methods. It should be noted that there are no FEM investigations for solving free surface problems related to cylindrical coordinates. In this work, the formulation and boundary conditions used for both FEM and FDM are identical. Therefore, as in the FDM formulation, full consideration of the surface tension effect along with normal and tangential stress conditions on the free surface are used for the FEM. The numerical procedure used in the present work is the Galerkin-based weighted residual method of finite element formulation. This work provides a critical quantitative and qualitative investigation of both methods applied to the free surface problems in cylindrical coordinates.

MATHEMATICAL FORMULATION

The governing equations and assumptions for the present study are similar to those presented in the work of Vafai and Chen [1]. The assumptions made in the present study are (1) incompressible flow, (2) axisymmetric flow, (3) viscosity and surface tension coefficients taken to be constant, and (4) gravitational effect neglected. The axis-symmetrical continuity and momentum in polar coordinates can then be represented as follows:

Continuity equation

$$\frac{1}{r}\frac{\partial}{\partial r}(ru) + \frac{\partial v}{\partial z} = 0 \tag{1}$$

Momentum equation

$$\frac{\partial u}{\partial t} + \frac{1}{r}\frac{\partial}{\partial r}(ru^2) + \frac{\partial uv}{\partial z} = -\frac{\partial \phi}{\partial r} + \nu\left[\frac{\partial}{\partial r}\left(\frac{1}{r}\frac{\partial}{\partial r}(ru)\right) + \frac{\partial^2 u}{\partial z^2}\right] \tag{2}$$

$$\frac{\partial v}{\partial t} + \frac{1}{r}\frac{\partial}{\partial r}(ruv) + \frac{\partial v^2}{\partial z} = -\frac{\partial \phi}{\partial z} + g + \nu\left[\frac{\partial}{\partial r}\left(\frac{1}{r}\frac{\partial}{\partial r}(rv)\right) + \frac{\partial^2 v}{\partial z^2}\right] \tag{3}$$

where $\phi = p/\rho$.

The required initial condition and boundary conditions for the velocity and pressure fields are discussed in the next section.

Initial Conditions

Based on physical considerations, the initial conditions are taken as zero velocity field and uniform pressure field. These initial conditions are similar to those used in the work of Vafai and Chen [1] and provide the velocity and pressure fields at the beginning of the computational scheme for Eqs. (2) and (3).

Boundary Conditions

Two types of boundary conditions are used in the present study. One is the boundary condition at the rigid wall, namely, the top and bottom boundaries of the hollow ampule, and the other is the boundary condition at the free surface. In the present study, no-slip conditions are used at the top and bottom rigid walls. For the free surface boundary condition, the tangential stress at the free surfaces and the normal stress at the free surface must exactly balance any externally applied normal stress. Balance between the normal stress and the externally applied normal stress is employed as the boundary condition in the present study. For the inner and outer free surfaces, the above mentioned boundary conditions can be written as follows.

On η

$$\phi_\eta = \phi_i - \frac{\sigma}{\rho}\kappa_\eta + 2\nu\left[n_r^2\frac{\partial u}{\partial r} + n_r n_z\left(\frac{\partial u}{\partial z} + \frac{\partial v}{\partial r}\right) + n_z^2\frac{\partial v}{\partial z}\right]_\eta \tag{4}$$

On ξ

$$\phi_\xi = \frac{\sigma}{\rho}\kappa_\xi + 2\nu\left[n_r^2\frac{\partial u}{\partial r} + n_r n_z\left(\frac{\partial u}{\partial z} + \frac{\partial v}{\partial r}\right) + n_z^2\frac{\partial v}{\partial z}\right]_\xi \tag{5}$$

Finite Element Formulation

Detailed discussions regarding the discretization of the governing equations and boundary conditions for FDM, including the free surface boundary conditions, were presented in the work of Vafai and Chen [1]. The work presented in this section will mainly stress the formulation of the FEM.

A Galerkin-based FEM was employed to solve the system of governing equations. The application of this technique is described by Taylor and Hood [4] and Gresho et al. [5], and its application in the finite element code used in the present work is also well documented [6]. This scheme is briefly explained here.

The domain under consideration is first divided into a set of simply shaped, nonoverlapping regions called elements, within each of which the unknown variables u_r, u_z, and p are approximated by using the following equations:

$$u_z \approx u_z^h = \phi^T[U_z] \tag{6}$$

$$u_r \approx u_r^h = \phi^T[U_r] \tag{7}$$

$$p \approx p^h = \psi^T[P] \tag{8}$$

where ϕ and ψ are the interpolation functions for velocity and pressure, respectively. These are local functions of the nodal coordinates for that element as well as the independent variables. The vectors $[U_z]$, $[U_r]$, and $[P]$ consist of the values of the respective variables at the nodes of that element.

For problems involving free surface boundaries, a different type of element is used on the inner and outer surface boundaries to account for the effect of the free surface. In the present study, a three-node triangular element is used on the free surface, and a nine-node quadratic element is used for the rest of the computational domain.

Substituting these basis functions into the governing equations and boundary conditions yields a residual (error) in each of the equations. This can be stated as follows:

Continuity

$$f_1(\phi, U_r, U_z) = E_1 \tag{9}$$

Momentum

$$f_2(\phi, \psi, U_r, U_z, P) = E_2 \tag{10}$$

where E_1 and E_2 are the residuals (errors) resulting from the use of the finite element approximations.

The Galerkin form of the method of weighted residuals seeks to reduce these errors to zero in a weighted sense, i.e., by making the residuals orthogonal to the interpolation functions of each element. These orthogonality conditions are expressed by

$$\int_v \psi \cdot E_1 dV = \int_v \psi \cdot f_1 dV = 0 \tag{11}$$

$$\int_v \phi \cdot E_2 dV = \int_v \phi \cdot f_2 dV = 0 \tag{12}$$

This procedure yields a system of equations for each element, which can be written as

$$\overline{M}\frac{\partial V}{\partial t} + \overline{K}(V) \cdot V = \overline{F} \tag{13}$$

where V is the column vector of the unknown variables, F is the force vector (incorporating the boundary conditions), M is the mass matrix, and K is the stiffness matrix (representing the diffusion and convection of energy).

The above equation represents the discrete analog of the governing continuum equations for an individual fluid element. The discrete representation of the entire continuum region of interest is obtained through an assemblage of elements such that interelement continuity of velocity and temperature is enforced. The result of such an assembly process is a system of matrix equations of the form given by Eq. (13).

To obtain a transient solution, the time dependent terms need to be replaced over a small portion of the problem time scale. It is an incremental procedure that advances the solution in discrete steps of time. Implicit and explicit time integration methods are two general approaches used in FDM and FEM to discretize the time dependent terms. As was discussed in [1], a semi-implicit scheme was employed in the FDM. Because it is a scheme with conditional stability, stability criterion had to be satisfied, resulting in a smaller time increment. For the present study, the trapezoidal implicit scheme developed by Gresho et al. [5] is used for the time discretization of the governing equations. Detailed derivation and discussion are presented in Ref. [6].

In the semi-implicit scheme used by Vafai and Chen [1], the pressure field was solved at each iteration, and the successive overrelaxation method was used to solve the pressure field equations. For the present study, since an implicit time integrator has been used for discretization of the governing equations in time, at each time step, a nonlinear system of equations including all field variables needs to be solved. Gresho et al. [5] showed that with the predictor-corrector scheme

used in the present code [6], if the user specified local time truncation error tolerance is set to 0.1–0.5% error, the predictor is sufficiently accurate that only one or two Newton-Raphson iterations are required at each time step to achieve convergence. This, however, can be very expensive in studies like the present case, for which even one iteration can take a considerable amount of CPU time when the Newton-Raphson method is used. To overcome this problem, a quasi-Newton solution algorithm is used to solve the nonlinear system at each time step. The description of this method is given by Engelman et al. [7]. This algorithm can be shown to be superlinearly convergent, and in practice, its convergence rate approaches that of the Newton-Raphson, while the time for one iteration of quasi-Newton is typically 10–20% of the time for a Newton-Raphson iteration. The advantage of the quasi-Newton method is that the reformation of the Jacobian matrix need only be performed every N time steps. Of course, a balance must be found between the number of steps N and the quasi-Newton iterations required at each time step to achieve convergence. Typically, if $N = 2$ or 3, a savings in computer time of the order of 50% over the one-step Newton-Raphson method can be attained.

Free Surface Formulation

The MAC method associated with irregular cells on the free surface was used to cope with the free surface boundary condition for the FDM. In the FEM, for each node at the free surface, a new degree of freedom is introduced for determination of the position of the free surface node within the region.

In the FEM, initial coordinates for nodes located at the free surfaces have to be specified, and special boundary elements for the free surfaces are also specified. The kinematic condition and cubic spline technique, which are the same approaches used in the finite difference scheme by Vafai and Chen [1], are employed in the finite element scheme to update the positions for nodes at both the inner and outer free surfaces and update curvature values for the boundary conditions at both free surfaces. Using the techniques mentioned above and applying the Galerkin finite element method to the governing equations plus the free surface boundary conditions, Eqs. (4) and (5), the matrix system of nonlinear algebraic equations for the free surface can be expressed as follows:

$$A(U)U + K(U)U - CP + BX = F \tag{14}$$

$$C^T U = 0 \tag{15}$$

$$K_n U = 0 \tag{16}$$

where X is the global vector of the free surface unknowns, $A(U)$ is the matrix that represents the contribution from the convective terms, $K(U)$ is the matrix that includes the diffusive terms, C is the divergence matrix, B is the matrix representing the contribution of the normal stress balance boundary condition in the momentum equation, K_n contains the normal velocity boundary condition effects, and F is the vector including the effects of surface stresses and contact angle

boundary conditions. The solver used for the FEM in the present work is the one described in Ref. [6].

RESULTS AND DISCUSSION

In the present work, a comparative study of finite difference and finite element solutions for the problem of free surface transport within a hollow ampule is presented. In addition to presenting the basic differences between the finite difference and finite element results, the effects of different radii ratio and different pressure differences on the FDM and FEM results are also investigated. The temporal variations for inner and outer radii for a given pressure difference are presented for two main cases. For case 1 the inner radius is taken as 0.1 m and the outer radius is set to 0.15 m, and for case 2 the inner radius is taken as 0.05 m and outer radius is set to 0.1 m. This results in a radii ratio of 1.5 for case 1 and of 2 for case 2.

An in-depth investigation on the effects of the number and the type of elements/nodes and the time increment has been performed. Preliminary tests to check the validity for the finite element scheme were made by using different time increments and by varying the number of elements. Extensive sets of numerical experiments were done to ensure that any further refinements in the number of elements/grids or any further reductions in the time increment as well as different types of elements (for the finite element method) would have no effect on the FDM and FEM results. For the FEM a trapezoid time integration scheme was used to discretize the time dependent terms in the governing equations. The trapezoid scheme facilitates taking larger time increments, since it is a second-order implicit scheme. Since a rigorous verification of the FDM algorithm is presented in Vafai and Chen [1], only the results of the verification for the FEM are presented in here. Figure 2 shows the FEM results for the temporal variations of the inner free surface of a hollow glass ampule with $R_i = 0.1$ m and outer radius of $R_o = 0.15$ m using three different time increments (0.1, 0.05, and 0.0255 s). It is apparent from Fig. 2 that any further reductions in the time increment will have very little influence on the variations of the inner free surface. Some limited results are presented in Fig. 3 for the extensive set of runs that were performed regarding the effects of the number of the elements in the r and z directions. These results are presented for the temporal variations of the inner free surface of a glass ampule with $R_i = 0.1$ m and $R_o = 0.15$ m using 31×11, 31×15, 31×21, and 31×25 mesh distributions in the z direction (Fig. 3). For brevity, the effects of the variations in the r direction are not shown in here.

A critical comparison of the FDM and FEM results is shown in Figs. 4–6 for two different radii ratios at a given pressure difference. Figure 4 presents the temporal variations of the inner radius obtained by FEM and FDM for a hollow ampule with $R_i = 0.1$ m and $R_o = 0.15$ m. Figures 5 and 6 present the inner and outer free surface variations for a hollow ampule with $R_i = 0.05$ m and $R_o = 0.1$ m. Qualitatively and quantitatively the results for the temporal variations of the outer free surface for case 1 were quite similar to the inner free surface variations shown in Fig. 4. For brevity, those results are not shown here. For both cases, 31 nodes in the radial direction and 11 nodes in the axial direction were chosen. The

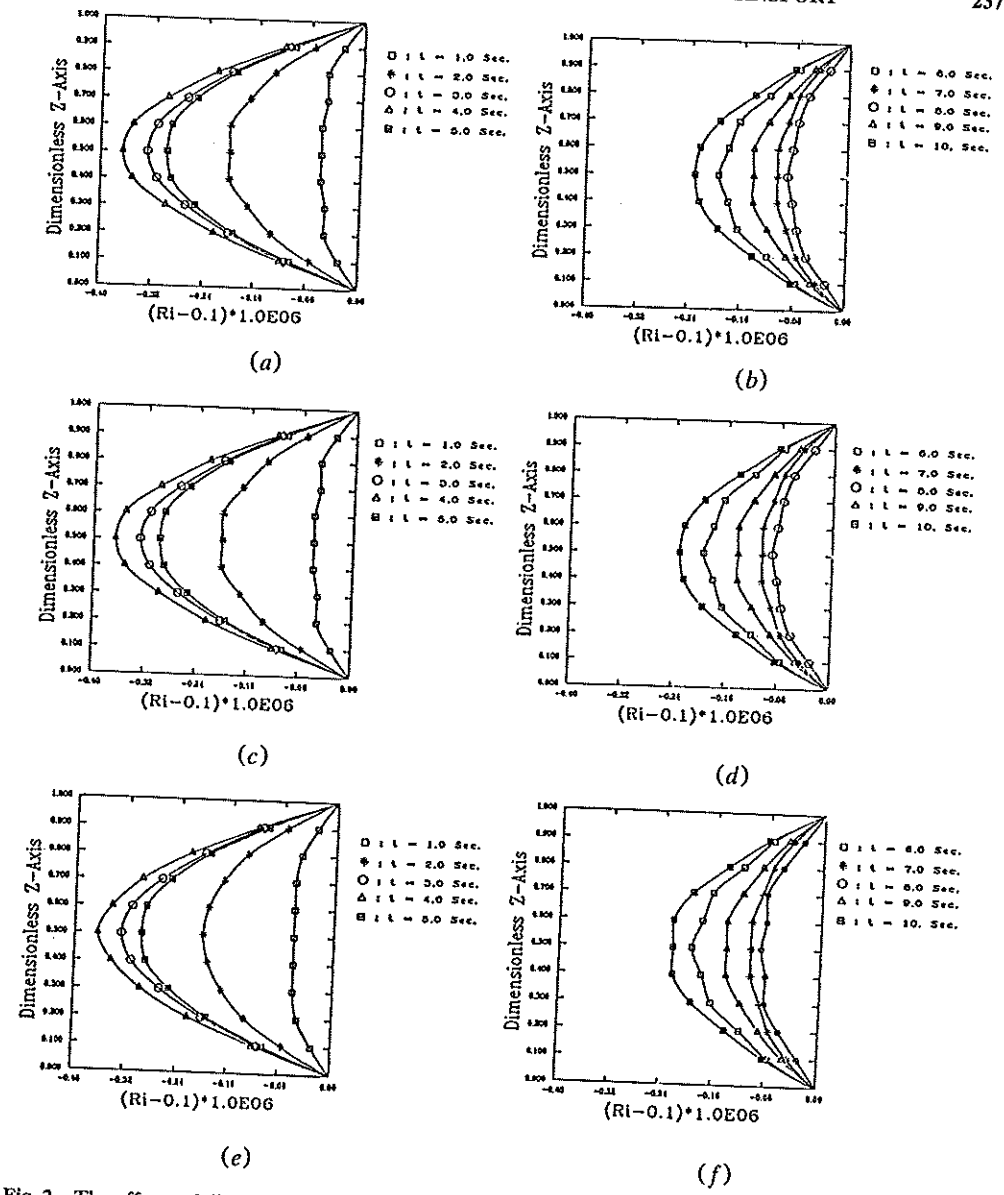

Fig. 2 The effects of different time increments on the temporal variations of the inner free surface of a hollow ampule for FEM runs with $R_i = 0.1$ m and $R_o = 0.15$ m with $\Delta P = 10^{-5}$: (*a*, *b*) $\Delta t = 0.025$ s; (*c*, *d*) $\Delta t = 0.05$ s; and (*e*, *f*) $\Delta t = 0.1$ s.

time increment was equal to 0.001 s for FDM and 0.1 s for FEM. The pressure difference across the film for Figs. 4–6 is equal to 10^{-5} Pa. For example, this pressure can be induced by various heating sources striking the outer free surface of a hollow ampule. As discussed earlier, comprehensive numerical experimentation was done to ensure that both the FDM and FEM results are independent of

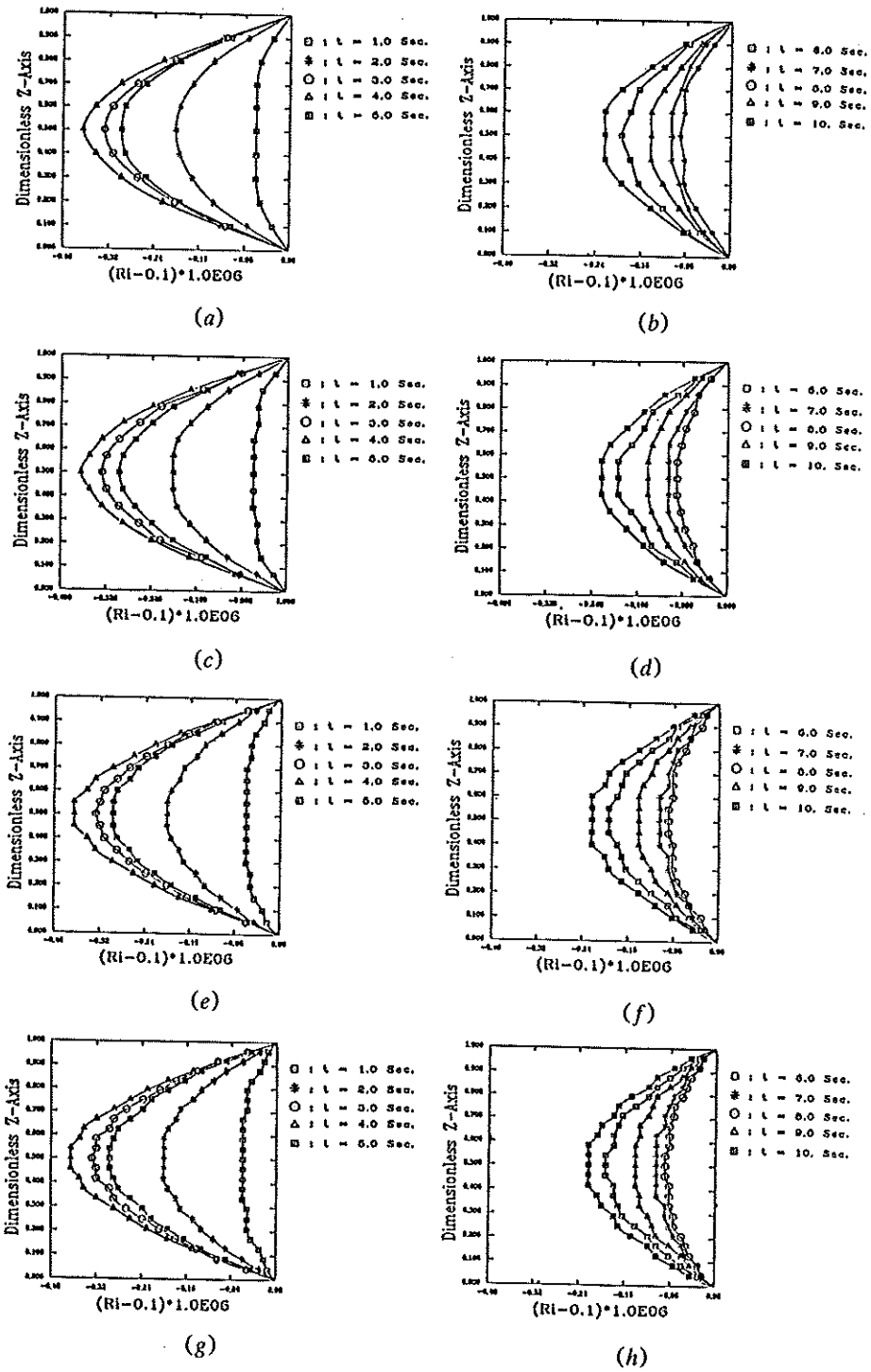

Fig. 3 The effects of number of elements on the temporal variations of the inner free surface of a hollow ampule for FEM runs with $R_i = 0.1$ m and $R_o = 0.15$ m with $\Delta P = 10^{-5}$: (*a*, *b*) 31 × 11; (*c*, *d*) 31 × 15; (*e*, *f*) 31 × 21; and (*g*, *h*) 31 × 25.

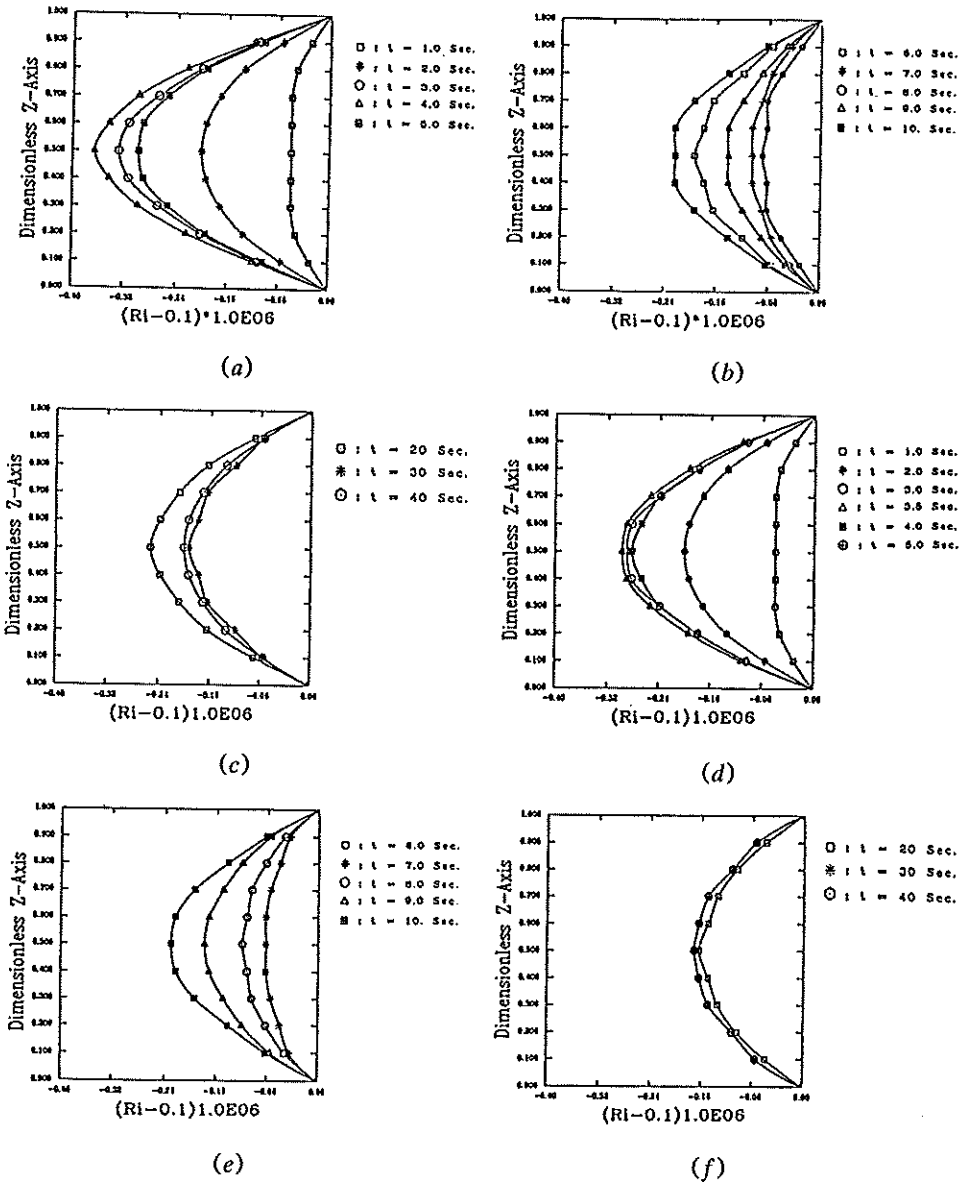

Fig. 4 Comparisons between FDM and FEM simulations for the temporal variations of the inner free surface of a hollow ampule for case 1 with $R_i = 0.1$ m and $R_o = 0.15$ m with $\Delta P = 10^{-5}$: (*a*, *b*, *c*) FEM and (*d*, *e*, *f*) FDM.

the grid size and the time increment. Furthermore, in the case of the FEM the results were independent of the type of the element chosen for the computational domain.

As seen in Figs. 4–6, for both the FEM and FDM simulations, initially the hollow ampule starts moving inward due to the applied pressure difference across the thickness of the hollow ampule. The same type of inward motion was also

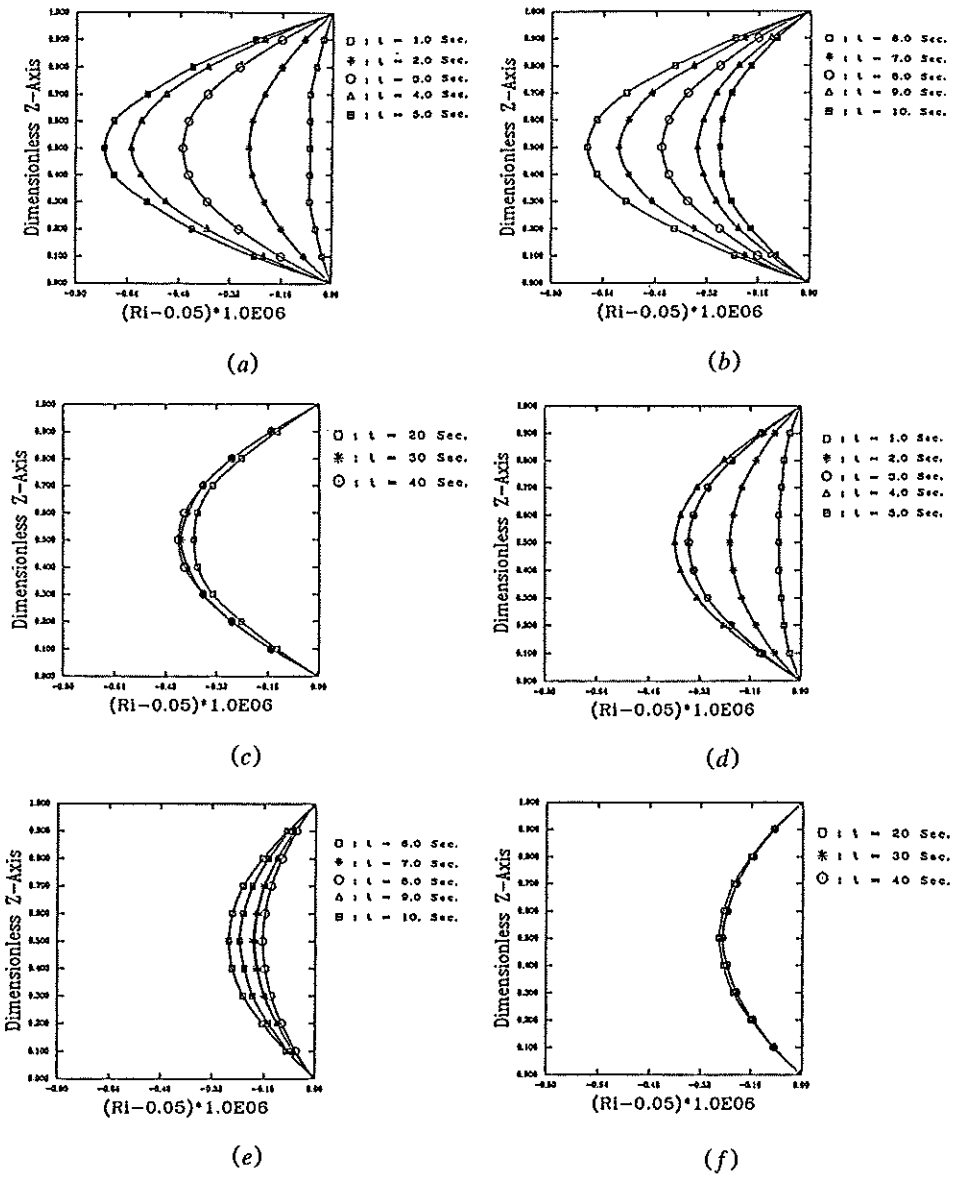

Fig. 5 Comparisons between FDM and FEM simulations for the temporal variations of the inner free surface of a hollow ampule for case 2 with $R_i = 0.05$ m and $R_o = 0.1$ m with $\Delta P = 10^{-5}$: (*a*, *b*, *c*) FEM and (*d*, *e*, *f*) FDM.

observed in the work of Chen and Vafai [8]. The results presented in Fig. 4 are for case 1, and the results presented in Figs. 5 and 6 are for case 2. The FEM results for case 1 are shown in Figs. 4*a*–4*c*, and the corresponding FDM results are shown in Figs. 4*d*–4*f*. As it can be seen from the FEM results, the inner free surface of the vertical film starts moving inward in about 4 s. However, after 4 s, due to the

dominance of the surface tension effects, the inward motion of the inner free surface stops, and the vertical film starts bouncing back and moving outward. For later times, other motion reversals occur at 8, 10, 20, and 30 s after the start of the process, leading toward the final steady state when a uniform pressure field is reached at 40 s. From the FDM simulations for the same process shown in Figs.

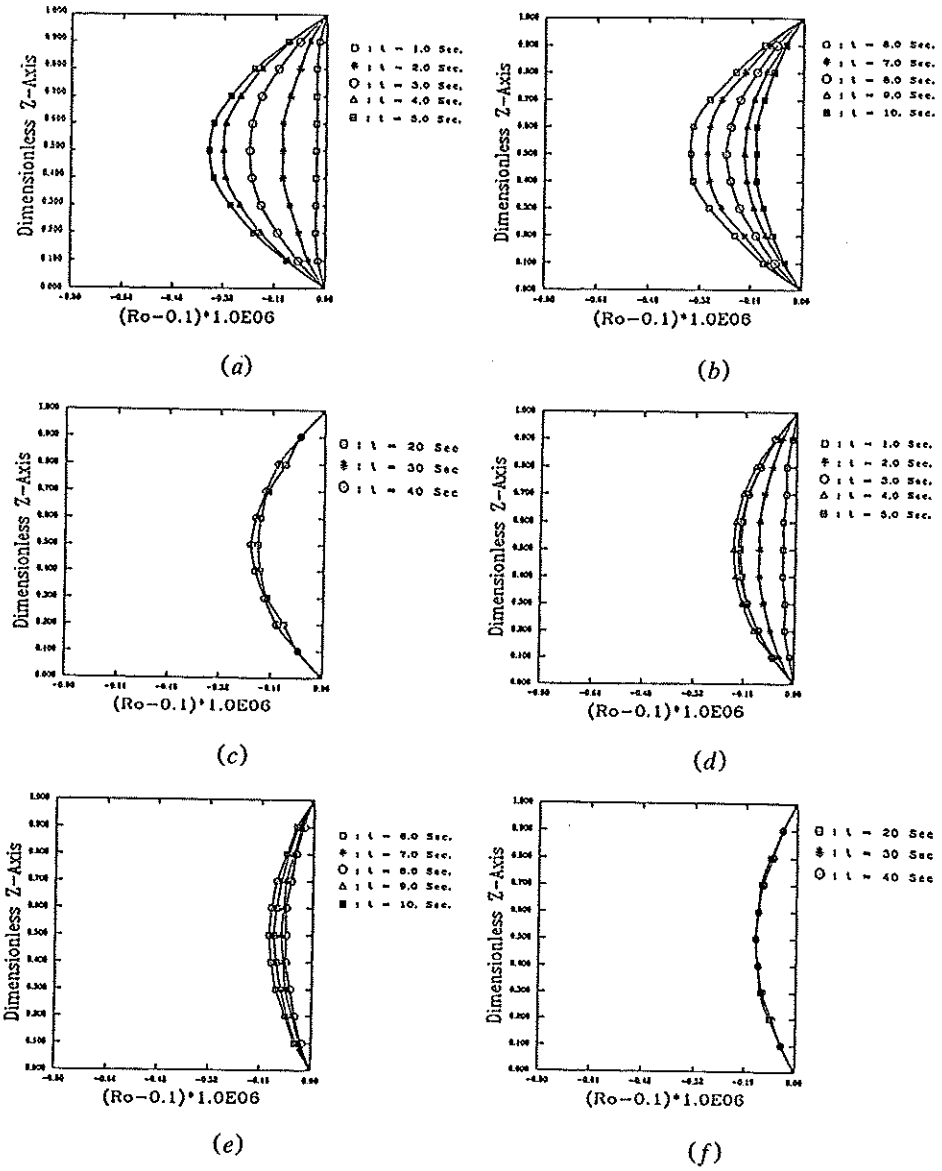

Fig. 6 Comparisons between FDM and FEM simulations for the temporal vanations of the outer free surface of a hollow ampule for case 2 with $R_i = 0.05$ m and $R_o = 0.1$ m with $\Delta P = 10^{-5}$: (*a*, *b*, *c*) FEM and (*d*, *e*, *f*) FDM.

4*d*–4*f* these motion reversals occurs at 3.5, 7, 10, and 20 s, and steady state is reached at 30 s. For both methods the motion reversal times for the outer free surface were found to be the same as those for the inner free surface. It is clear from these comparisons that the FDM and FEM results match very well up to the first 3 s from the start of the process. For later times, qualitatively, the results from both simulations are in very good agreement. However, there are quantitative discrepancies between the results obtained by the FEM and FDM simulations. Detailed information for comparisons between the motion reversal times as well as the required time for reaching steady state are listed in Table 1. It should be emphasized again that both the FEM and FDM results presented in this work were independent of grid size and time increment.

Temporal variations of the inner and outer free surfaces for case 2 with a radii ratio of 2 and the same applied pressure as in case 1 are shown in Figs. 5 and 6. Here again for the initial 3 s, results obtained by FEM and FDM simulations are very close. However, as in case 1, for later times the FEM results predict larger free surface deformations than the FDM results. Detailed information for comparisons between the motion reversal times as well as the required time for reaching steady state conditions for the inner and outer free surfaces is listed in Tables 2 and 3, respectively. As in case 1, for both methods the motion reversal times for the outer free surface were found to be the same as those for the inner free surface. For the FDM simulation, the first motion reversal for both free surfaces appears at 4.0 s, while the corresponding motion reversal for the FEM simulation occurs at 5 s. The second motion reversal, occurs at 10 s for FEM and at 8 s for FDM simulations. Eventually, as expected, both methods predict that the film does come to rest. The steady state conditions are reached after 30 s for FEM runs, while the FDM runs predict that steady state conditions are reached after 20 s.

As can be seen in Figs. 4–6 the FEM and FDM comparative results display similar qualitative phenomena as well as the same number of motion reversals. The quantitative differences, such as different motion reversal times and magnitudes of free surface deformations, are attributed to the inherent differences in approaches used in the FEM and FDM formulations. As mentioned earlier, great care was taken to ensure that both the FDM and FEM results are independent of grid size, element type (for FEM), and time increment. It should be noted that the results obtained by both methods satisfy exactly the same governing equations, boundary conditions, and initial conditions. However, it is the inherently different discretization schemes used in the FDM and FEM simulations that leads to different solution matrices and results in the subsequent quantitative differences.

Table 1 Motion Reversal Times for the Inner Free Surface for a Hollow Ampule with $R_i = 0.1$ m and $R_o = 0.15$ m

Numerical scheme	Reversal motion, s				
	First	Second	Third	Fourth	Steady State
FEM	4.0	8	10	30	40
FDM	3.5	7	10	20	30

Table 2 Motion Reversal Times for the Inner Free Surface for a Hollow Ampule with $R_i = 0.05$ m and $R_o = 0.1$ m

Numerical scheme	Reversal motion, s		
	First	Second	Steady State
FEM	5.0	10	30
FDM	4.0	8	20

After some extensive investigations, it was established that for a given radii ratio corresponding to a given set of geometric dimensions, for either FDM or FEM, the motion reversal times are independent of the applied pressure difference across the thickness of the hollow ampule. Figure 7 presents the FDM results for case 1 for three applied pressure differences (10^{-5}, 10^{-3}, 10^{-1}) for a hollow ampule with $R_i = 0.1$ m and $R_o = 0.15$ m. As can be seen from Fig. 7, the driving force (applied pressure difference) has essentially a direct linear relationship with the magnitude of the free surface deformation. That is a 100-fold increase in the magnitude of the applied pressure difference across the hollow ampule results in exactly the same order of magnitude increase in the magnitude of the free surface deformation. However, as can be seen from Fig. 7, the motion reversal times are independent of the applied pressure differences. Therefore, in Fig. 7, the first and second reversals occur at 3.5 and 7 s, respectively, regardless of the magnitude of the driving force.

Figures 8 and 9 show the effects of different driving forces for case 2 for the FDM and FEM simulations, respectively. Clearly, exactly the same conclusions stated earlier in connection with Fig. 7 apply for both of these figures. That is, for any radii ratio, for either method, the applied pressure difference has a direct linear effect on the magnitude of the free surface deformations and no effect on the motion reversal times. This interesting property allows prediction of the free surface deformations and motion reversal times for different magnitudes of the driving pressure difference, for either FDM or FEM simulations, once the results for a given radii ratio corresponding to a given set of geometric dimensions are known. This type of property can lead to significant CPU savings for free surface investigations related to various applications.

Table 3 Motion Reversal Times for the Outer Free Surface for a Hollow Ampule with $R_i = 0.05$ m and $R_o = 0.1$ m

Numerical scheme	Reversal motion, s		
	First	Second	Steady State
FEM	5.0	10	30
FDM	4.0	8	20

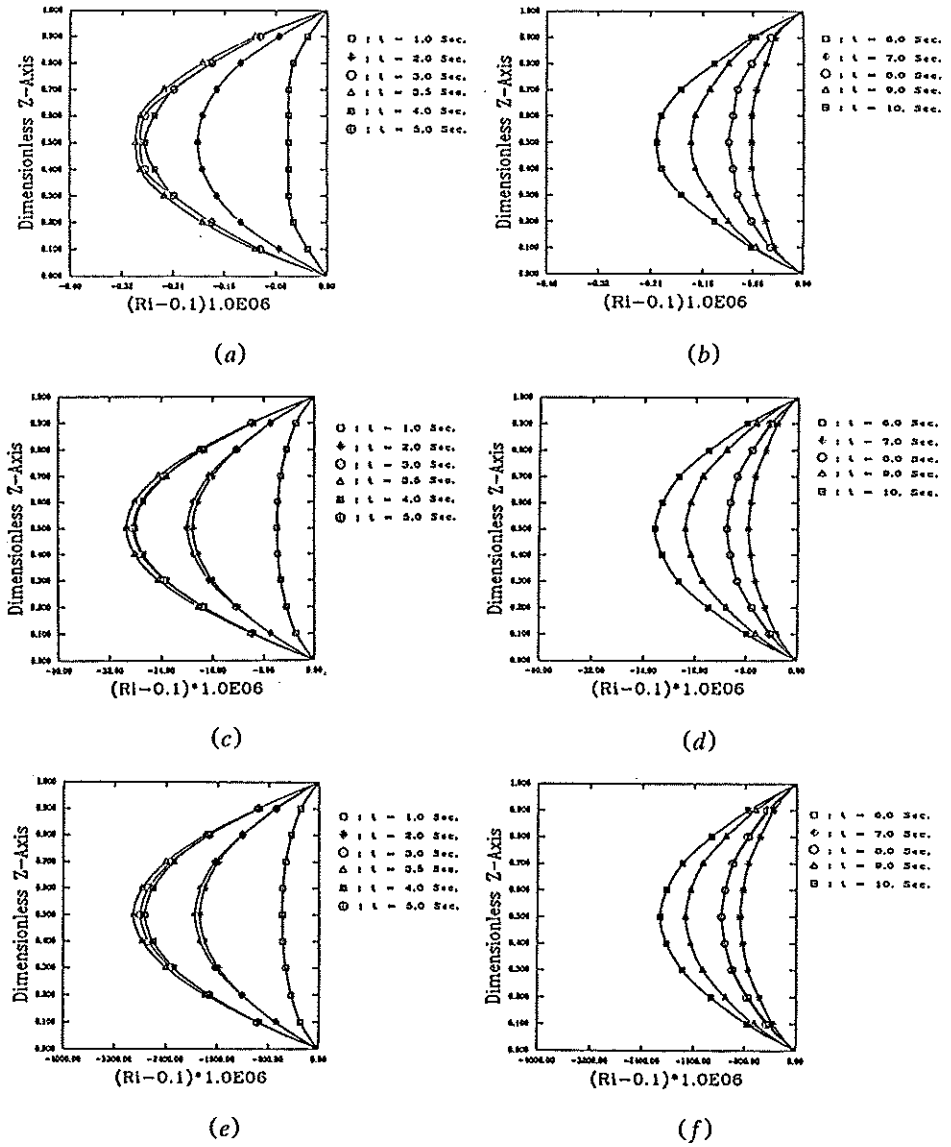

Fig. 7 Effects of the applied pressure difference across the thickness of the hollow ampule on the temporal inner free surface variations for the FDM simulations for case 1 with $R_i = 0.1$ m and $R_o = 0.15$ m: (*a*, *b*) $\Delta P = 10^{-5}$; (*c*, *d*) $\Delta P = 10^{-3}$; (*e*, *f*) $\Delta P = 10^{-1}$.

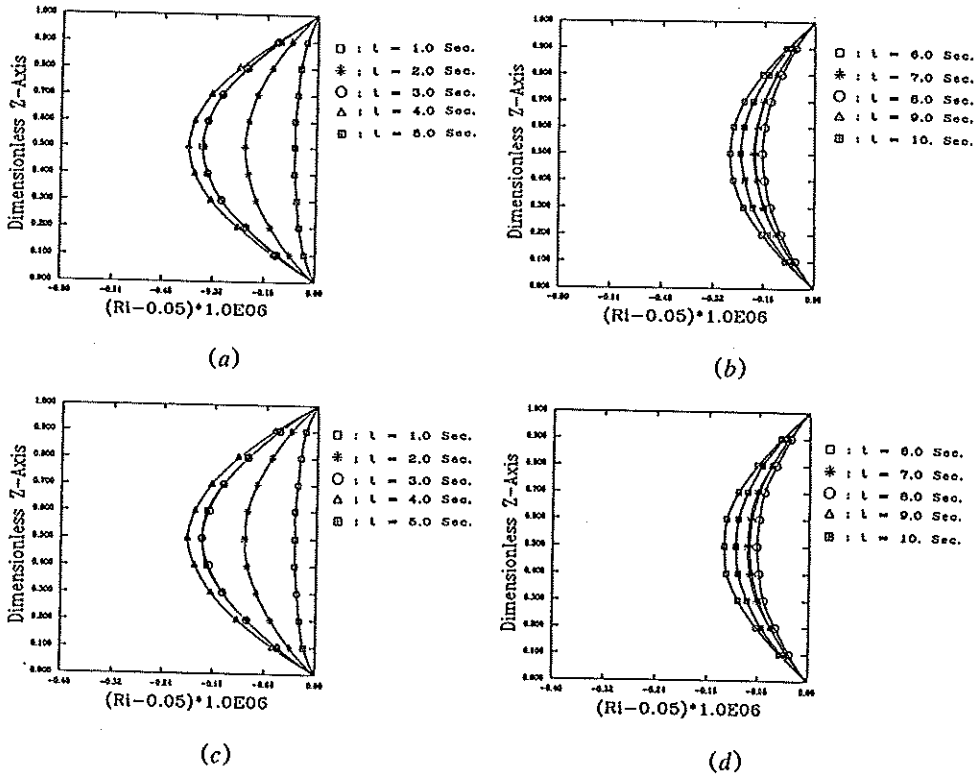

Fig. 8 Effects of the applied pressure difference across the thickness of the hollow ampule on the temporal inner free surface variations for the FDM simulations for case 2 with $R_i = 0.05$ m and $R_o = 0.1$ m: (*a*, *b*) $\Delta P = 10^{-5}$ and (*c*, *d*) $\Delta P = 10^{-6}$.

CONCLUSIONS

The present work consists of an in-depth comparative analysis for finite difference and finite element methods as related to free surface transport phenomena. Exactly the same governing equations, boundary conditions, and initial conditions were employed in both the FEM and FDM simulations. A critical comparison shows that the FEM and FDM results are both qualitatively and quantitatively very close during the earlier times, while for later times, qualitatively, the results from both simulations are in very good agreement. However, there are quantitative discrepancies between the results obtained by the FEM and FDM simulations. The quantitative differences, such as different motion reversal times and magnitudes of free surface deformations, are attributed to the inherent differences in the approaches used in the FEM and FDM formulations. It is established that for any radii ratio, for either method, the applied pressure difference has a direct linear effect on the magnitude of the free surface deformations and no effect on the

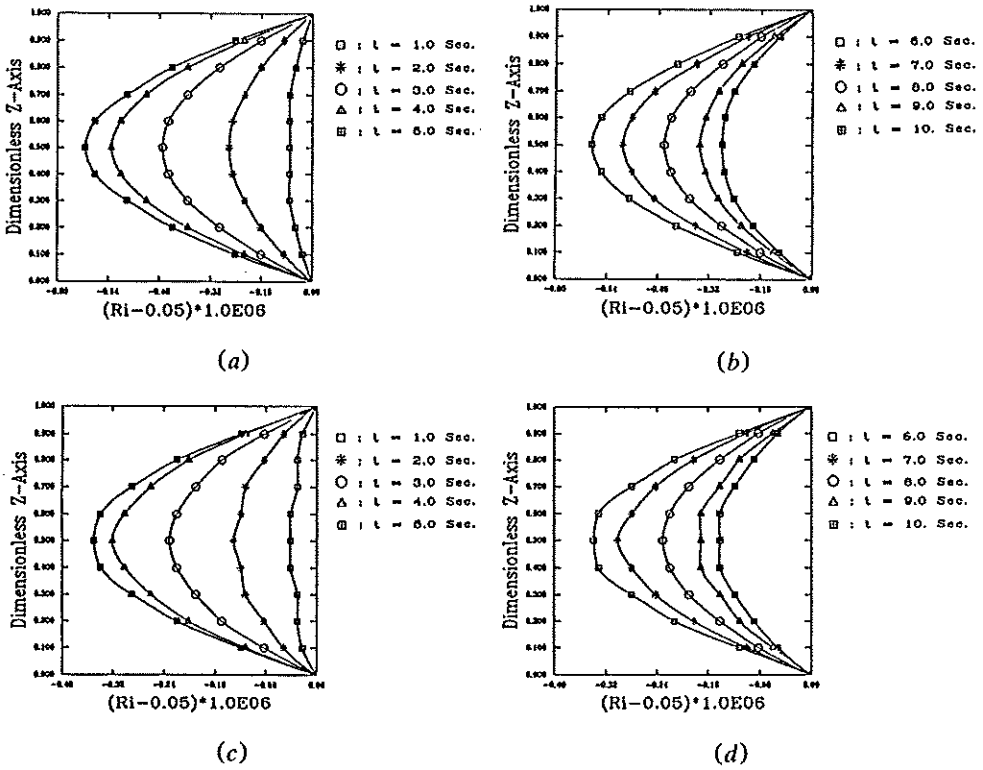

Fig. 9 Effects of the applied pressure difference across the thickness of the hollow ampule on the temporal inner free surface variations for the FEM simulations for case 2 with $R_i = 0.05$ m and $R_o = 0.1$ m: (*a*, *b*) $\Delta P = 10^{-5}$ and (*c*, *d*) $\Delta P = 5.0 \times 10^{-6}$.

motion reversal times. This property can lead to significant CPU savings for various applications related to free surface transport.

REFERENCES

1. K. Vafai and S. C. Chen, Analysis of Free Surface Transport within a Hollow Glass Ampule, *Numer. Heat Transfer, Part A*, vol. 22, pp. 21–49, 1992.
2. E. R. G. Eckert and Robert M. Drake, Jr., *Analysis of Heat and Mass Transfer*, McGraw-Hill, New York, 1972.
3. H. P. Wang, Free Surface Modeling of a Glass Tube Sealing Process, *ASME Winter Annual Meeting PED*, vol. 13, pp. 361–370, 1984.
4. C. Taylor and P. Hood, A Numerical Solution of the Navier-Stokes Equations Using the Finite Element Technique, *Comput. Fluids*, vol. 1, pp. 73–89, 1973.
5. P. M. Gresho, R. L. Lee, and R. L. Sani, On the Time-Dependent Solution of the Incompressible Navier-Stokes Equations in Two and Three Dimensions, in *Recent Advances in Numerical Methods in Fluids*, Pineridge, Swansea, England, 1980.

6. Fluid Dynamics International, *FIDAP Theoretical Manual*, 1990.
7. M. S. Engelman, G. Strang, and K. J. Bathe, The Application of Quasi-Newton Methods in Fluid Mechanics, *Int. J. Numer. Meth. Eng.*, vol. 17, pp. 707–718, 1981.
8. S. C. Chen and K. Vafai, An Experimental Investigation of free Surface Transport, Bifurcation, and Adhesion Phenomena as Related to a Hollow Glass Ampule and Metallic Conductor, *J. Heat Transfer*, vol. 114, pp. 743–751, 1992.

Received 3 March 1992
Accepted 30 April 1992

Address correspondence to K. Vafai.